Three-dimensional visualization of magnetization reversal behavior inside a high-performance Nd–Fe–B permanent magnet

Technological innovation is strongly required in various fields to achieve carbon neutrality by 2050. To this goal, materials science and material development technology can significantly contribute. For example, high-performance permanent magnets are one of the essential materials for developing environmental and energy-saving technologies, which are used in driving motors for electric vehicles, compressors for air conditioners, wind power generators, and other applications. Further improvement in the magnetic properties of permanent magnet materials, such as coercivity and maximum energy product, can improve the energy efficiency of the environmentally important applications above.

Coercivity is one of the most important measures of magnet performance. Materials with higher coercivity are harder to reverse their magnetization to maintain a strong magnetic force even under high demagnetization fields and high-temperature environments, such as inside a driving motor housing. Moreover, coercivity is closely related to another characteristic called magnetic hysteresis in the magnetization curve. In general, permanent magnet materials have a wide hysteresis loop and, correspondingly, a high coercivity. Nd–Fe–B is a typical material with considerable magnetic hysteresis to exhibit high coercivity as a strong permanent magnet.

Consequently, the development of permanent magnet materials is aimed at increasing the magnetic hysteresis and coercivity further to achieve ultimate performance that exceeds that of currently used Nd–Fe–B magnets. Even though coercivity is a fundamental property of permanent magnets, the mechanism that causes high coercivity has remained unresolved for more than 100 years since the start of magnetism research. It is necessary to clarify the mechanism of high coercivity to develop permanent magnet materials with excellent performance.

One key to understanding the coercivity mechanism is the material's microstructure. Nd–Fe–B sintered magnets are made by sintering $Nd_2Fe_{14}B$ grains with diameters of a few microns or less. The material has a microstructure that consists of $Nd_2Fe_{14}B$ main phase grains, Nd-rich phases containing metallic Nd and Nd oxides of different compositions, and a grain boundary phase containing alloys of Fe, Nd, Cu, and other rare-earth elements. The macroscopic magnetic properties of a bulk Nd–Fe–B magnet are the sum of the magnetization of millions of $Nd_2Fe_{14}B$ grains. Therefore, the microscopic coercivity mechanism can be understood if the magnetization reversal process of individual internal grains can be observed. For this purpose, magnetic microscopy studies have been performed on Nd–Fe–B magnets using different magnetic imaging techniques, including magneto-optical Kerr microscopy (MOKE), magnetic force microscopy (MFM), magnetic scanning electron microscopy (magnetic SEM), scanning X-ray transmission microscopy (STXM), and photoemission electron microscopy (PEEM). However, these conventional magnetic imaging techniques are only applied to the sample surface to obtain two-dimensional (2D) magnetization distribution images, namely, magnetic domains in 2D. They cannot be used to obtain three-dimensional (3D) images of internal magnetic domains.

Recently, several research groups have developed a 3D magnetic microscopy technique called X-ray magnetic tomography [1-4]. In X-ray magnetic tomography measurement, a number of 2D projection images with magnetic contrasts using X-ray magnetic circular dichroism (XMCD) are taken at different sample rotation angles. Then, a dedicated reconstruction algorithm is applied to the magnetic projection data to obtain a 3D image of the magnetization distribution inside the sample. At SPring-8 **BL39XU**, a scanning hard X-ray magnetic tomography technique has been developed [1]. This technique has enabled 3D magnetic domain imaging with a spatial resolution of 360 nm, and the observation is possible under a magnetic field of 1 T.

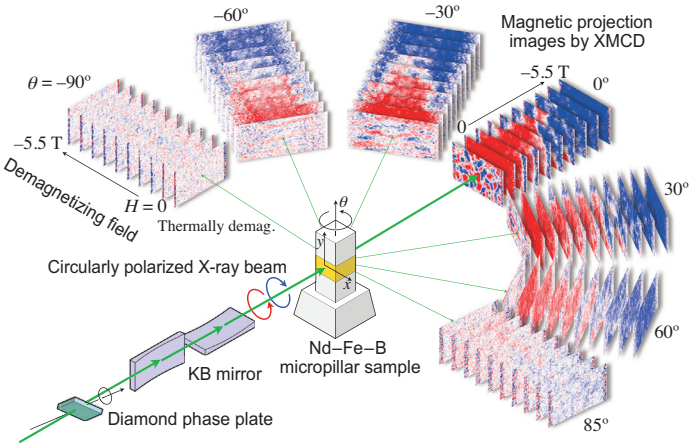

Fig. 1. Schematic of scanning hard X-ray magnetic tomography measurements of high-performance permanent magnet, performed at SPring-8 BL39XU.

In this study, we applied the X-ray magnetic tomography technique to a high-performance permanent magnet material to directly observe magnetic domain structures inside a bulk sample in 3D [5]. Figure 1 shows a schematic of our experiment. The sample was a state-of-the-art fine-grained Nd–Fe–B sintered magnet fabricated by pressless sintering and grain boundary diffusion processes with Tb–Cu eutectic alloy. Its average grain diameter is ~1 μm and its coercivity was 2.7 T. A bulk sample was fabricated into a micropillar with dimensions of 18×18×50 μm^3 by a focused ion beam technique. To study the evolution of internal magnetic domains during the demagnetization process, we used an offline electromagnet and a superconducting magnet to apply a high magnetic field. The sample was initially fully magnetized by applying a +5.5 T field along the easy magnetization direction (parallel to the *c*-axis). X-ray magnetic tomography measurement was performed at the remanent state after the demagnetizing field was applied to the sample, and it was repeated with increasing demagnetizing field from 0 to –5.5 T across the coercivity of 2.7 T.

Figure 2(a) shows the reconstructed 3D density map showing the microstructure and magnetic domain structure in the same observation area of 18×18×10 μm^3, which contains about 4000 grains. The high resolution microstructure image was obtained by 3D scanning electron microscopy (3D-SEM) with by the corresponding image from conventional X-ray tomography, while the magnetic domain image was obtained by X-ray magnetic tomography measurement at the Nd L_2 edge. These 3D images allow us to determine the correlation between the internal microstructure and magnetic domains. Figure 2(b) demonstrates the variation of the internal magnetic domain structures at different demagnetizing fields along the hysteresis curve. We successfully visualized the magnetization reversal behavior of individual magnetic grains with a diameter of ~1 μm. By carefully examining the correlation between the variation of magnetic domains and the microstructure, we have identified some grains that serve as the intrinsic nucleation and annihilation sites of magnetic domains, namely, the departing and terminating points of magnetization reversal, respectively. Moreover, unexpected behaviors of local magnetic domains have been observed, such as magnetic domains formed by chains of reversed magnetic grains connecting perpendicularly to the easy magnetization direction and grains whose magnetization reverses back against the demagnetizing field increase. These unnatural behaviors of the local magnetic domains are probably due to a reformation of the magnetic domains caused by a significant change in the local magnetostatic interaction field.

In summary, our X-ray magnetic tomography study demonstrated an actual microscopic picture of the magnetization reversal behavior in high-performance Nd–Fe–B permanent magnets. The results can provide information useful for clarifying the coercivity mechanism. The observed 3D magnetic and microstructural images will be used as an excellent model in micromagnetic simulations based on our practical experiment to improve calculation accuracy and reliability. The results of this study will open new doors to the study and design of new permanent magnet materials.

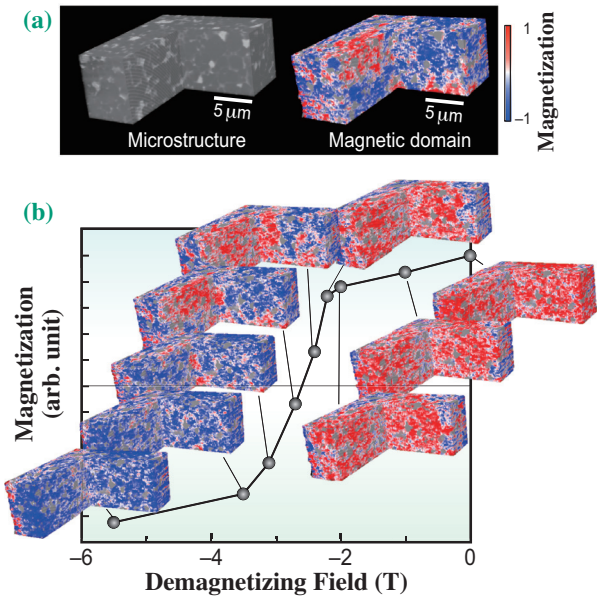

Fig. 2. Three-dimensional reconstructed images of **(a)** microstructure (left) and magnetic domain structure (right) inside a fine-grained Nd–Fe–B sintered magnet. **(b)** Variation of the magnetic domain structure as a function of demagnetizing field along the magnetic hysteresis curve [5].

Motohiro Suzuki[a,*] and Satoshi Okamoto[b]

[a] School of Engineering, Kwansei Gakuin University
[b] Institute of Multidisciplinary Research for Advanced Materials (IMRAM), Tohoku University

* Email: m-suzuki@kwansei.ac.jp

References

[1] M. Suzuki *et al.*: Appl. Phys. Express **11** (2018) 036601.
[2] C. Donnelly *et al.*: Nature **547** (2017) 328.
[3] A. Hierro-Rodríguez *et al.*: Nat. Comm. **11** (2020) 1.
[4] S. Seki *et al.*: Nat. Mater. **21** (2022) 181.
[5] *M. Takeuchi, M. Suzuki, S. Kobayashi, Y. Kotani, T. Nakamura, N. Kikuchi, A. Bolyachkin, H. Sepehri-Amin, T. Ohkubo, K. Hono, Y. Une and S. Okamoto: NPG Asia Mater.* ***14*** *(2022) 70.*